



ELSEVIER

Physica D 74 (1994) 90–106

PHYSICA D

The Eckhaus instability in hexagonal patterns

M.M. Sushchik, L.S. Tsimring

Institute for Nonlinear Science, University of California, San Diego, CA 92093-0402, USA

Received 24 June 1993; revised 18 November 1993; accepted 24 November 1993

Communicated by A.C. Newell

Abstract

The Eckhaus instability of hexagonal patterns is studied within the model of three coupled envelope equations for the underlying roll systems. The regions of instability in the parameter space are found analytically from both the phase approximation and a full system of amplitude equations. Beyond the stability limits of hexagons two different modes go unstable. Both provide symmetry breaking of an initially regular pattern via splitting of a triplet of rolls into two triplets of growing disturbances. The parameters of fastest growing disturbances (wavelength, orientation, growth rate) are determined from the full set of linearized amplitude equations. The nonlinear stage of the Eckhaus instability is investigated numerically. Symmetry breaking due to the Eckhaus instability indeed occurs within a certain range of parameters, which for small supercriticality parameter μ leads to a metastable disordered hexagonal state with numerous line and point defects. For larger μ the Eckhaus instability triggers the transition of regular hexagonal pattern to disordered roll state. The roll phase originates in the cores of defects and then spreads all over the pattern.

1. Introduction

Hexagonal patterns occur near the onset of cellular instabilities in a large variety of spatially extended nonequilibrium systems. Well-known examples are Rayleigh–Bénard convection in non-Boussinesq fluid [1–3], Bénard–Marangoni convection [4], Turing structures in chemical reactions [5,6], etc. (see also the review [7]). A perfect hexagonal pattern can be thought of as a superposition of three periodic waves (we will call them “rolls” as in convection) oriented at 120° with respect to each other with strictly synchronized phases of individual rolls (a sum of all three phases should be equal to zero for stable stationary hexagonal pattern). The problem of pattern selection arises in the case of hexagons exactly as in the case of striped systems. Indeed, for supercritical situation a finite band of wavenumbers goes unstable, and the period of rolls forming a hexagonal pattern can differ from an optimal wavenumber corresponding to the maximum of the growth rate of the primary instability. It is well known that one of the mechanisms determining the wavenumber selection in Boussinesq (roll) convection is the Eckhaus instability [10] resulting in the exponential growth of wavenumber modulations and, on the nonlinear stage, change of the initial wavenumber towards

the optimal value through the nucleation of defects. It appears natural that an analogous process should provide pattern selection in case of hexagonal patterns as well.

A perfect hexagonal pattern is a triplet of three roll systems $\mathcal{A}_i \exp(i\mathbf{q}_i \cdot \mathbf{r})$, $i = 1, 2, 3$, $\mathbf{r} = \{x, y\}$ with wavevectors $\mathbf{q}_{1,2,3}$ satisfying the three-wave resonance condition

$$\mathbf{q}_1 + \mathbf{q}_2 + \mathbf{q}_3 = 0,$$

and the wavenumbers of all three waves are equal and the phases are synchronized. (All \mathbf{q}_i and \mathbf{r} are normalized by an appropriate dimensional length scale of the system ξ_0 .) Let us introduce a small parameter ϵ which measures the distance from the threshold of primary instability $\epsilon = (R - R_c)/R_c$, where R is a control parameter (e.g. Rayleigh number), and R_c is its critical value. The amplitudes \mathcal{A}_i are all $\mathcal{O}(\epsilon^{1/2})$.

In the lowest order of ϵ , one can describe the evolution of perfect hexagonal patterns with optimal wavenumber q_0 (corresponding to the maximal growth rate of the primary instability) by the following system of three equations for the complex amplitudes of three roll systems:

$$\begin{aligned} \partial_t \mathcal{A}_i &= \epsilon \mathcal{A}_i + \alpha \mathcal{A}_j^* \mathcal{A}_k^* - (|\mathcal{A}_i|^2 + \gamma |\mathcal{A}_j|^2 + \gamma |\mathcal{A}_k|^2) \mathcal{A}_i, \\ \{i, j, k\} &= \{1, 2, 3\}, \quad \{2, 3, 1\}, \quad \{3, 1, 2\}. \end{aligned} \quad (1)$$

Here $\alpha = \mathcal{O}(\epsilon^{1/2})$ is the coefficient of quadratic nonlinearity, describing non-Boussinesq effects, and $\gamma = \mathcal{O}(1)$ is the ratio of the coefficient of cubic interaction of rolls of different orientation to the coefficient of cubic self-interaction. If $\alpha \neq 0$ we can rescale all variables such that the coefficients at the quadratic terms in (1) are equal to one, new supercriticality parameter $\mu = \epsilon/\alpha^2 = \mathcal{O}(1)$, and new amplitudes $A_i = \mathcal{A}_i/\alpha = \mathcal{O}(1)$.

Our goal will be to study the stability properties of the hexagonal patterns with $|\mathbf{q}_1| = |\mathbf{q}_2| = |\mathbf{q}_3| \neq q_0$. We shall denote $|q_i| - q_0 = k$. If $k = \mathcal{O}(\alpha, \epsilon^{1/2})$ one can still use the amplitude equations however with additional Newell–Whitehead–Segel-type terms describing smooth spatial evolution of the envelope [8,9,13–15]. In the new rescaled variables they read

$$\partial_t A_i = \mu A_i + A_j^* A_k^* - (|A_i|^2 + \gamma |A_j|^2 + \gamma |A_k|^2) A_i + \widehat{D}_i^2 A_i. \quad (2)$$

These differ from (1) by the linear terms $\widehat{D}_i^2 A_i$ in the right-hand sides. Here $\widehat{D}_i = iK + \partial_{X_i} - i\alpha/2q_0 \partial_{Y_i}^2$, $X_i = \alpha x_i$; $Y_i = \alpha y_i$ are pairs of rescaled dimensionless Cartesian coordinates orthogonal and parallel to rolls axes, respectively, and $K = k\alpha^{-1} = \mathcal{O}(1)$. The parallel diffusion (terms proportional to $\partial_{Y_i}^2$ in \widehat{D}_i) is usually much weaker than the transversal diffusion. In case of hexagonal patterns we have to assume the same scaling for both x_i and y_i coordinates and therefore cannot scale out the small parameter α from the amplitude Eqs. (2) unlike the case of roll patterns. In the following we always assume $\alpha/q_0 \rightarrow 0$, and subsequently $\widehat{D}_i \equiv iK + \partial_{X_i}$ if not explicitly stated otherwise.

The set of Eqs. (2) has a variational form

$$\partial_t A_i = -\frac{\delta \mathcal{F}}{\delta A_i^*},$$

with the free energy functional,

$$\begin{aligned} \mathcal{F} = \int dx dy [&-\mu (|A_1|^2 + |A_2|^2 + |A_3|^2) - (A_1^* A_2^* A_3^* + \text{c.c.}) + \frac{1}{2} (|A_1|^4 + |A_2|^4 + |A_3|^4) + \\ &\gamma (|A_1|^2 |A_2|^2 + |A_1|^2 |A_3|^2 + |A_2|^2 |A_3|^2) + (|\widehat{D}_1 A_1|^2 + |\widehat{D}_2 A_2|^2 + |\widehat{D}_3 A_3|^2)], \end{aligned} \quad (3)$$

so only static patterns can be expected as $t \rightarrow \infty$.

One can easily find all possible stationary homogeneous solutions of (2) (cf., for example, [3]):

$$(i) \text{ rolls } A_1 = (\mu - K^2)^{1/2}, \quad A_2 = A_3 = 0, \quad (4)$$

$$(ii) \text{ hexagons } A_1 = A_2 = A_3 = A_0 \equiv \left(1 \pm \sqrt{1 + 4(\mu - K^2)(1 + 2\gamma)} \right) / 2(1 + 2\gamma), \quad (5)$$

$$(iii) \text{ mixed states } A_1 = 1/(\gamma - 1), \quad A_2 = A_3 = \sqrt{(\mu - K^2 - A_1^2)/(1 + \gamma)} \quad (6)$$

and all permutations of indices $\{1,2,3\}$. The hexagonal solution corresponding to the ‘-’ sign in (5) is always unstable so in the following we will refer to the hexagons as the solution (5) with the ‘+’ sign only.

The rest of the paper is organized as follows. In Section 2 we perform the stability analysis of hexagonal solution (5) within the framework of the phase approximation which allows determination the stability limits of hexagons. Section 3 is devoted to the linear analysis of the Eckhaus instability for the full set of amplitude Eqs. (2). We compute parameters and structure of growing disturbances and predict symmetry breaking due to the Eckhaus instability. In Section 4 we perform numerical simulations of the Eckhaus instability within the system (2). The Eckhaus instability indeed leads to the symmetry breaking and appearance of domains with different orientations of hexagons (or rolls, in some region of parameter plane). These domains are separated by numerous line and point defects. Section 5 presents our conclusions.

2. Linear stability analysis. Phase approximation

Stability of hexagonal patterns has been studied starting from the pioneering papers by Segel [11] and Busse [12]. They considered the stability of perfect hexagonal patterns with $K = 0$ with respect to spatially homogeneous disturbances and found that hexagons are stable within the range $-1/4(1 + 2\gamma) < \mu < (\gamma + 2)/(\gamma - 1)^2$. Caroli et al. [13] and Malomed et al. [14] extended this analysis for the case of non-zero K and long-wave disturbances (non-dimensional wavenumber $Q \ll 1$). They deduced the stability limits from the 6th order dispersion relation after linearization the full system (2). Meanwhile, exactly the same formulas can be obtained more easily within so called phase approximation, namely under the assumption that the amplitudes adiabatically follow phase dynamics. This approximation is valid in the limit $Q \rightarrow 0$, i.e. precisely at the threshold of the instability (see Section 3).

Let us add small perturbations to the regular hexagonal pattern in the form

$$A_i = (A_0 + a_i) e^{i\phi_i}, \quad i = 1, 2, 3, \quad (7)$$

where $a_i(\mathbf{r}, t), |\nabla\phi_i(\mathbf{r}, t)| \ll 1$. Substitution of (7) into (2) and linearizing with respect to small perturbations of amplitudes and phases give rise to the following set of equations:

$$\partial_t a_i = -[(1 + 2A_0)A_0 - \partial_{x_i}^2]a_i + (A_0 - 2\gamma A_0)A_0(a_j + a_k) - 2KA_0\partial_{x_i}\phi_i, \quad (8)$$

$$\partial_t \phi_i = (-A_0 + \partial_{x_i}^2)\phi_i - A_0(\phi_j + \phi_k) + 2KA_0^{-1}\partial_{x_i}a_i. \quad (9)$$

For long-wave perturbations in the region of parameters where hexagons are stable with respect to spatially homogeneous disturbances, time and space derivatives of amplitudes a_i in (8) are of the

higher order in Q and can be neglected. Then (8) yields linear algebraic relations between a_i and phase gradients $\partial_{X_i}\phi_i$:

$$a_i = \lambda \partial_{X_i}\phi_i + \beta \partial_{X_j}\phi_j + \beta \partial_{X_k}\phi_k, \quad (10)$$

where $\lambda = c(1 - b)/(b + 1)(b + 2)$, $\beta = -c/(b + 1)(b - 2)$, $b = (2A_0 + 1)/(1 - 2\gamma A_0)$, $c = 2K/(1 - 2\gamma A_0)$. After substituting (10) into (9) one can get the system of phase equations

$$\partial_t \phi_i = -A_0(\phi_i + \phi_j + \phi_k) + (1 + 2K\lambda)\partial_{X_i}^2 \phi_i + 2K\beta \partial_{X_i}\partial_{X_j}\phi_j + 2K\beta \partial_{X_i}\partial_{X_k}\phi_k. \quad (11)$$

Substitution of the plane wave solution $\phi_i \sim \exp(i\mathbf{Q}\mathbf{R} + \omega t)$ ($\mathbf{R} = \{X, Y\}$) yields the cubic dispersion relation of interest

$$\omega^3 + g_2\omega^2 + g_1\omega + g_0 = 0, \quad (12)$$

where

$$\begin{aligned} g_0 &= \frac{9}{16} [(1 + 2K\lambda)^2 - 4K^2\beta^2] A_0 Q^4 + \mathcal{O}(Q^6), \\ g_1 &= \frac{9}{16} [(1 + 2K\lambda)^2 - 4K^2\beta^2] Q^4 + 3(1 + 2K\lambda + K\beta) A_0 Q^2, \\ g_2 &= 3[A_0 + (1 + 2K\lambda)Q^2/2]. \end{aligned}$$

Thus, the phase approximation enabled us to reduce the order of dispersion relation down to three, and now one can find the solution in the explicit form. It is interesting that the coefficients $g_{1,2,3}$ are independent of the direction of the vector \mathbf{Q} in the lowest order of Q (only in this order is the phase approximation justified), and therefore the growth rate is the same for any direction of \mathbf{Q} (see also [13,14]). As we shall see in the next section, the angular dependence does appear in the full set of six equations at $Q \sim 1$, and there are well-defined directions of the maximal growth of disturbances. This will give rise to the symmetry breaking on the nonlinear stage of the Eckhaus instability. It is easy to see that all three roots of dispersion relation (12), $\omega_{1,2,3}$, are real (the matrix of the eigenvalue problem is Hermitian), one root (ω_3) is always negative and the other two can change the sign. Since $g_2 \geq 0$, the stability region is simply determined by condition $g_0 \geq 0$ (and, of course, $K^2 \geq 0$), which yield the following set of inequalities:

$$\mu \leq \frac{1}{2}A_0(3A_0 - 1 + 3A_0\gamma), \quad \text{if } A_0 \geq 1/2\gamma, \quad (13)$$

$$\mu \leq -\frac{A_0(-6A_0^2 + A_0 - 10A_0^2\gamma + 3 - 9\gamma A_0 + 4\gamma^2 A_0^2)}{4A_0 + 2}, \quad \text{if } A_0 \leq 1/2\gamma, \quad (14)$$

$$K^2 \equiv \mu - (1 + 2\gamma)A_0^2 + A_0 \geq 0. \quad (15)$$

(All these formulas, as well as those to follow, have been checked with the MAPLE V symbolic computation program.) One can verify that stability conditions (13)–(15) coincide with those derived from the full set of amplitude equations in the limit $Q \rightarrow 0$ [14]. We find it more convenient to draw the stability limits in the (K, μ) parameter plane. Fig. 1 exemplifies the "stability balloon" for $\gamma = 2$. Line 1 represents the boundary of the region of existence of hexagons, namely,

$$K^2 = \mu + \frac{1}{4(1 + 2\gamma)}. \quad (16)$$

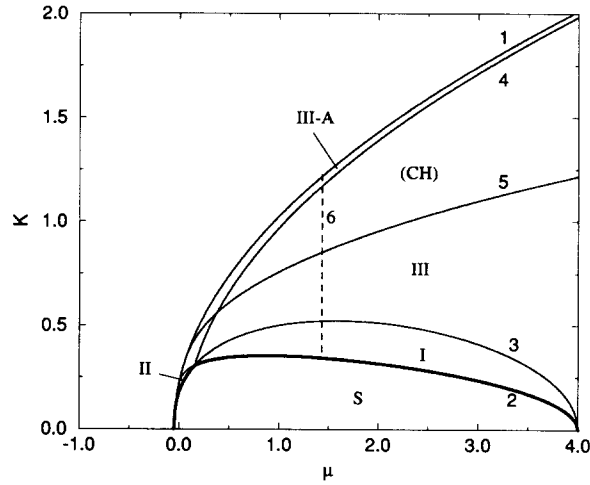


Fig. 1. Stability limits for Eckhaus instability of hexagons at $\gamma = 2$. Line 1 (Eq. (16)) limits the region of existence of hexagons, above the lines 2 and 3 two different roots of the dispersion relation (12) become positive (bold parts of them limit the band of stable hexagons). Line 4 separates the regions III of “wide splitting” instability where $\omega_m(0) > \omega_m(\pi/6)$ (below), and III-A of “narrow splitting” instability where the inequality is the opposite (above). Line 5 (Eq. (23)) is a lower boundary of the “cross-hexagon” (CH) instability, and to the right of the line 6 transition to a roll pattern takes place as a final result of Eckhaus instability of hexagons (see Section 4 below).

The coefficient g_0 turns into zero on lines 2 and 3. Line 2 where $\beta - \lambda = 1/2K$, is described by the formula

$$K^2 = \frac{1}{4} \left(1 + 4\mu + 8\gamma\mu - \frac{(-\gamma - 2 + (1 + 2\gamma) \sqrt{24\mu(1 + \gamma) + 1})^2}{9(1 + \gamma)^2} \right) (1 + 2\gamma)^{-1}. \quad (17)$$

We have an explicit formula for line 3 where $\beta + \lambda = -1/2K$, as well, however it is too long to reproduce in the paper. As one can see (Fig. 1), the region of stability (S) lies inside the region of existence of hexagons and, unlike the case of roll convection, is closed (at large enough $\mu > (\gamma + 2)/(\gamma - 1)^2$ hexagons are unstable even for zero K). Outside this region hexagons are unstable, in the region (I) or (II) the eigenvalue ω_1 or ω_2 becomes positive, respectively, and in the region (III) they both are positive, that means the two different modes go unstable simultaneously.

The next natural step is to determine the characteristics of the growing disturbances. However, within the phase approximation we cannot explore the instability region far from the threshold lines, because if the wavenumber Q_{\max} at which the growth rate reaches the maximum is not small as compared to 1, the phase approximation breaks down.

3. Linear stability analysis of the full system

In this section we study the full set of linearized Eqs. (8), (9). The dispersion equation that determines the the growth rate ω can be written in the form

$$\begin{vmatrix} \Lambda_{11} - \omega & \Lambda_{12} & \Lambda_{12} & \Lambda_{14} & 0 & 0 \\ \Lambda_{12} & \Lambda_{22} - \omega & \Lambda_{12} & 0 & \Lambda_{25} & 0 \\ \Lambda_{12} & \Lambda_{12} & \Lambda_{33} - \omega & 0 & 0 & \Lambda_{36} \\ \Lambda_{14}^* & 0 & 0 & \Lambda_{44} - \omega & \Lambda_{45} & \Lambda_{45} \\ 0 & \Lambda_{25}^* & 0 & \Lambda_{45} & \Lambda_{55} - \omega & \Lambda_{45} \\ 0 & 0 & \Lambda_{36}^* & \Lambda_{45} & \Lambda_{45} & \Lambda_{66} - \omega \end{vmatrix} = 0, \quad (18)$$

where

$$\begin{aligned} \Lambda_{ii} &= -(1 + 2A_0)A_0 - Q_i^2, \quad i = 1, 2, 3, \\ \Lambda_{ii} &= -A_0 - Q_i^2, \quad i = 4, 5, 6, \\ \Lambda_{12} &= (1 - 2\gamma A_0)A_0, \quad \Lambda_{45} = -A_0, \\ \Lambda_{14} &= -i2KQ_1, \quad \Lambda_{25} = -i2KQ_2, \quad \Lambda_{36} = -i2KQ_3, \\ Q_1 &= Q \cos \theta, \\ Q_2 &= -\frac{1}{2}Q(\cos \theta + \sqrt{3} \sin \theta), \\ Q_3 &= -\frac{1}{2}Q(\cos \theta - \sqrt{3} \sin \theta). \end{aligned} \quad (19)$$

$$(20)$$

Here Q and θ are the magnitude and angle of the wavevector \mathbf{Q} with respect to the direction of \mathbf{q}_1 .

Analysis of the stability conditions within the framework of the full dispersion relation (18) gives precisely the same results as the phase approximation (13)–(15) because these conditions are determined by the long-wave limit $Q \rightarrow 0$, for which the phase approximation is exact. Let us now look at the parameters of growing disturbances inside the instability region.

For each combination of parameters K , μ , Q , and θ there are six eigenvalues $\{\omega_i, i = 1, \dots, 6\}$, and each value of the growth rate corresponds to a six-dimensional eigenvector $\mathbf{v} = \{a^1, a^2, a^3, \phi^1, \phi^2, \phi^3\}$. Again, the matrix in (18) is Hermitian, so all eigenvalues are always real. It turns out that only two of them may become positive. We found it useful to plot simultaneously isolines of the growth rate $\omega_m = \max\{\omega_i, i = 1, \dots, 6\}$ over a gray-scaled distribution of the magnitude of the corresponding eigenvector component $|\phi^1|$ on the parameter plane $\{Q, \theta\}$ ¹. One example of this diagram is shown in Fig. 2a for $K = 0.45, \mu = 0.6$ (in this and all the following numerical examples we shall take $\gamma = 2$). These K and μ belong to the region I in Fig. 1. In this case only one root ω_1 of the dispersion Eq. (18) is positive, so $\omega_m \equiv \omega_1$. For $Q \ll 1$ the growth rate does not depend on θ in accordance with the phase approximation analysis. However, this dependence does appear at $Q \sim 1$. As one could expect, due to the hexagonal symmetry and the reflectional symmetry of Eqs. (8), (9) in \mathbf{Q} -space the growth rate is even and periodic in θ with the period $\pi/3$. The maximum growth rate is reached at some $Q_{\max} \simeq 0.75$ and $\theta_{\max} = n\pi/3$ ². Distribution of $|\phi^1|$ (shown in gray scale in Fig. 2a) is periodic with the period π . Along the line $Q = Q_{\max}$ it reaches 0 at $\theta = 0, \pi$ and reaches its maximum at $\theta = \pm\pi/2$. This distribution of ϕ^1 indicates that only components with $\theta = \pm\pi/3, \pm 2\pi/3$ are excited since $\phi^1(0) \simeq 0$ (similarly, $a^1(0) \simeq 0$). As we shall see in the next section, at the nonlinear stage an “up-down” symmetry $\omega_m(\theta) = \omega_m(\pi - \theta)$ is broken and the

¹ Two other phase components ϕ^2, ϕ^3 can be found from ϕ^1 since $\phi^2(Q, \theta) = \phi^1(Q, \theta + 2\pi/3)$ and $\phi^3(Q, \theta) = \phi^1(Q, \theta - 2\pi/3)$ due to hexagonal symmetry. The amplitude components a^1, a^2, a^3 have qualitatively similar structure and we do not show them here.

² If terms $\mathcal{O}(\alpha)$ describing parallel diffusion are kept, reflection symmetry of the amplitude Eqs. (2) is broken, and the growth rate is periodic with the period $2\pi/3$, and the angles of maximal growth rate slightly differ from $n\pi/3$.

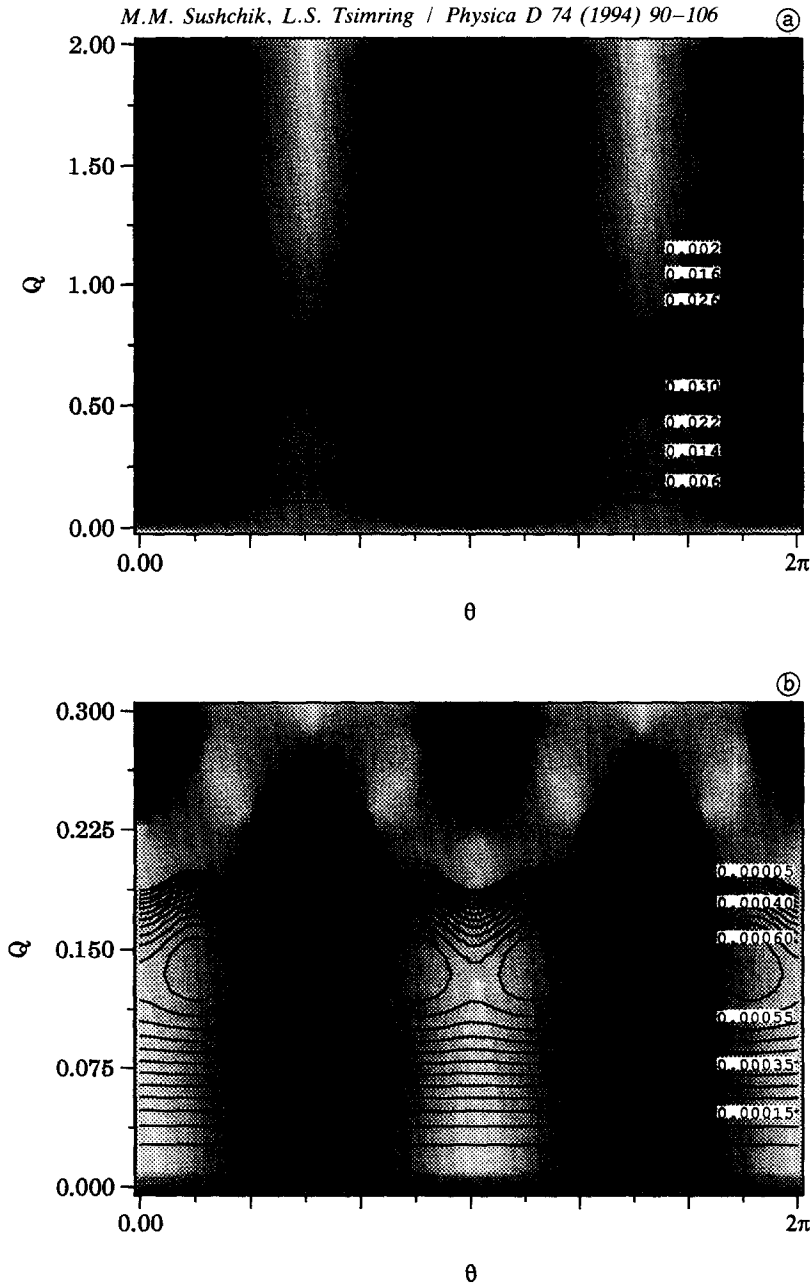
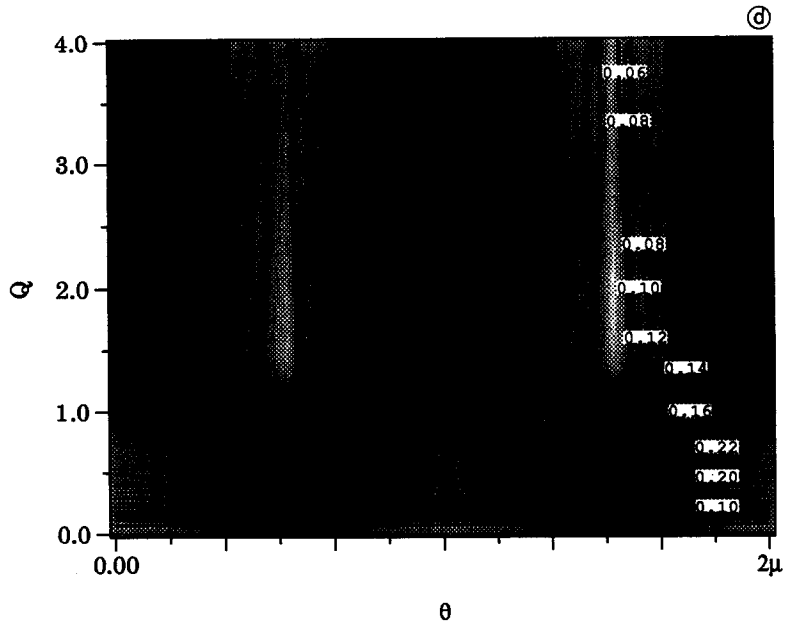
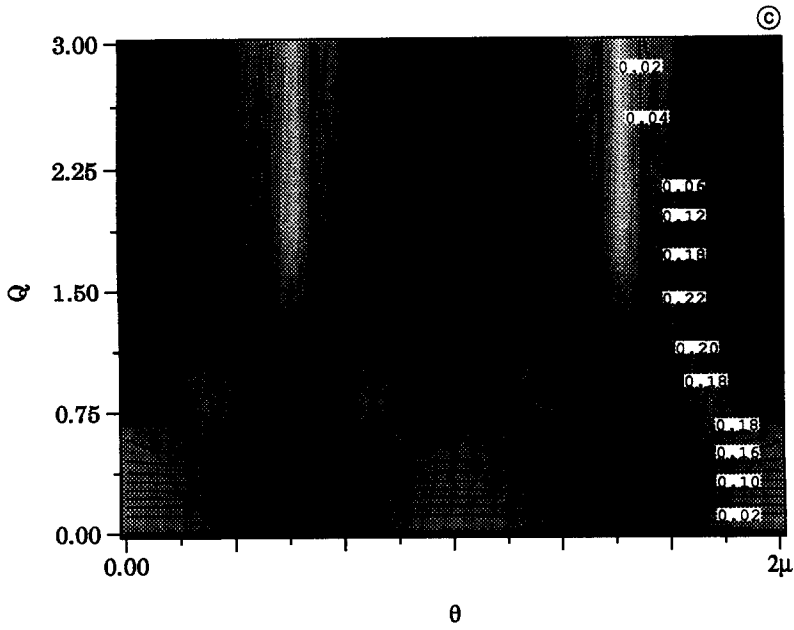


Fig. 2. Isolines of the maximal growth rate of small disturbances overlaid with the gray scale distributions of the component ϕ^1 of the corresponding eigenvector in the plane (Q, θ) at different K and μ ($\gamma = 2$): (a) $K = 0.45, \mu = 0.6$ (region I in Fig. 1), (b) $K = 0.28, \mu = 0.1$ (region II), (c) $K = 0.65, \mu = 0.6$ (region III), (d) $K = 0.56, \mu = 0.3$ (region III-A). Black color corresponds to $|\phi^1| = 0$, white to $|\phi^1| = 1$, only isolines with the positive values of the growth rate are shown.

pair of the wave components with wavenumbers closer to the optimal one outruns (in the case of positive K it corresponds to $\theta = \pm 2\pi/3$ and for negative K , $\theta = \pm \pi/3$, as shown schematically in Fig. 3a). This oblique excitation of long-wave disturbances will lead on the nonlinear stage to the symmetry breaking and development of domain structure with different orientation of hexagons (or rolls) inside the domains.



In the region II (Fig. 1) the second root ω_2 of the dispersion relation (18) becomes positive. The corresponding diagram of $\omega_2(Q, \theta)$ for $K = 0.28$ and $\mu = 0.1$ is presented in Fig. 2b. The most important difference from the previous case is that the maximum growth rate is reached now at $\theta = \pi/6 + \pi n/3$. Analysis of the eigenvectors corresponding to the maximal growth rate (gray scale distribution in Fig. 2b) shows that wave components with $\theta = \pm\pi/6, \pi \pm \pi/6$ have maximal magnitude. Therefore, again we have splitting into two triplets, however they have a smaller oblique angle (see sketch Fig. 3b). We will call the case of Fig. 3a “wide splitting”, and the case of Fig. 3b “narrow splitting”.

In the region III both modes grow simultaneously (there are two positive roots of (18)). Figs.

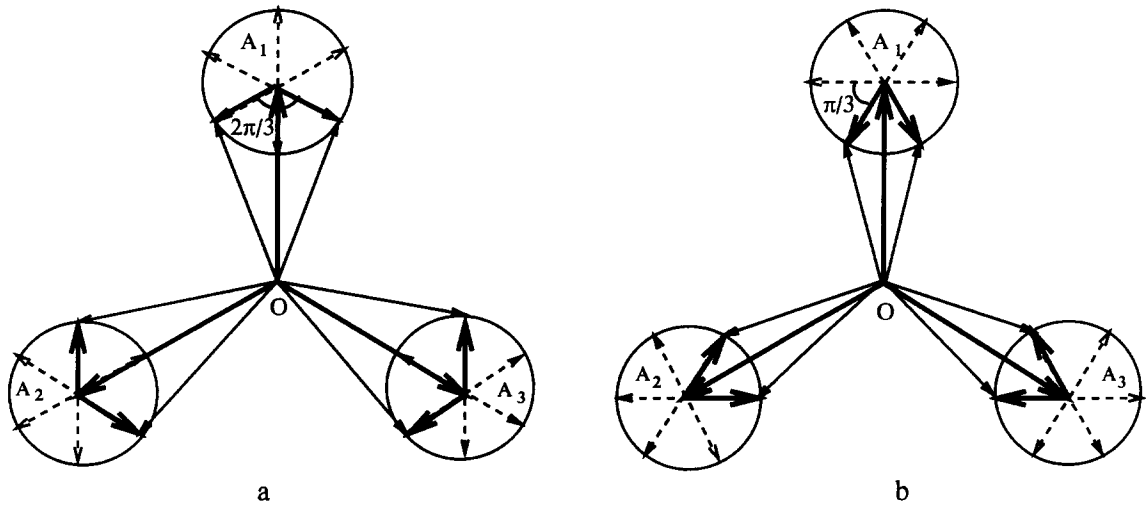


Fig. 3. Sketches of the wavevectors plane for the two different scenarios of Eckhaus instability: (a) “wide splitting” (cases (a), (c) of Fig. 2); (b) “narrow splitting” (cases (b), (d) of Fig. 2).

2c,d show $\omega_m(Q, \theta)$ for $K = 0.65$, $\mu = 0.6$ and $K = 0.56$, $\mu = 0.3$. In both cases there are maxima at both $\theta = \pi n/3$ and $\theta = \pi/6 + \pi n/3$, however, in the first case the magnitude of $\omega_m(n\pi/3) > \omega_m(\pi/6 + n\pi/3)$, and in the second the inequality is the opposite. One can be interested in the line where $\omega_m(n\pi/3) = \omega_m(\pi/6 + n\pi/3)$ in the plane (K, μ) . This line is shown in the Fig. 1 (line 4). For $\gamma = 2$ this line is described by a very simple formula

$$K = \sqrt{\mu - \frac{1}{16}}. \quad (21)$$

Below this line the triplets shown in Fig. 3a grow faster, and above it those of Fig. 3b prevail.

An interesting observation regarding Figs. 2c, d is that at some angles close to $\pi/6 + n\pi/3$ the growth rate remains positive at arbitrary large Q . The reason for this seemingly “spurious” behavior is quite clear. Consider for example the case $n = 1, 4$ for which the eigenvector ϕ^1 is nonzero. These angles correspond to directions in the \mathbf{q} -space orthogonal to the direction of the wavevector \mathbf{q}_1 . In the limit $k/q_0 \rightarrow 0$ ($\alpha \rightarrow 0$) that we have taken, the growth rate $\mu(\mathbf{q}) = \mu - (\mathbf{q} - \mathbf{q}_1)^2$ doesn't decay in the direction orthogonal to \mathbf{q}_1 , and therefore the diffusion term in the corresponding first amplitude equation turns into zero. Although the other two amplitude equations still have nonzero diffusion terms, the eigenvector of the growing disturbances has components $\phi^1 \gg \phi^2, \phi^3$ ($\phi^1(\pi/2) \gg \phi^1(\pi/2 \pm 2\pi/3), \phi^1(\pi/2 \pm \pi/3)$), so the dissipation due to $\phi^{2,3}$ is much less than amplification due to ϕ^1 . When small corrections $\mathcal{O}(\alpha)$ are taken into consideration, the region of positive ω is limited at finite (although large) $Q \sim q_0 \alpha^{-1}$. Although the growth rate of disturbances may be significant there, this region is of course beyond the validity of the amplitude description.

For large Q a simpler approach can be used to investigate the stability. In fact, one needs to explore the stability of the hexagonal pattern described by (1) against a different hexagonal pattern with an optimal wavenumber q_0 and an essentially different orientation, so the three-wave resonant interaction between two hexagonal patterns is absent. For this “cross-hexagon” (CH) instability (cf. “cross-roll” instability for the Boussinesq convection [16]), the linear equations for the small amplitudes of rolls forming a new hexagonal pattern read

$$\dot{b}_i = \mu b_i - 3\gamma|A_0|^2 b_i, \quad i = 1, 2, 3, \quad (22)$$

where A_0 is given by (5). The condition $\mu = 3\gamma|A_0|^2$ provides the boundary of the “cross-hexagon” instability

$$K^2 = \frac{(\gamma - 1)\mu + \sqrt{3\gamma\mu}}{3\gamma} \quad (23)$$

(see Fig. 1, line 5). However, it turns out that this cross-hexagon instability region lies inside the Eckhaus band, and the growth rate for that is lower than the maximal growth rate of the latter (at least, for the parameter values we used).

4. Numerical simulations

For numerical integration of Eq. (2) we employed a pseudo-spectral split-step method on a square mesh with the system size 64×64 or 128×128 and zero-gradient boundary conditions. We used the time step 0.1, the mesh size 0.5, and the parameter $\gamma = 2$. As initial conditions we take regular hexagonal patterns with non-optimal wavenumber and small additive random noise, that in terms of the amplitude Eqs. (2) means

$$A_i(x, y, 0) = A_0 + \xi(x, y), \quad i = 1, 2, 3, \quad (24)$$

where A_0 is described by (5), and $\langle \xi^2 \rangle \approx 10^{-4}$.

In our numerical experiments we investigated the nonlinear stage of the Eckhaus instability within the regions I, III, and III-A of the parameter plane (K, μ) (see Fig. 1). The growth rate in the region II is very small and we were unable to perform numerical simulations for the Eckhaus instability in that region.

In the first run we have taken $K = 0.45$ and $\mu = 0.6$ that corresponds to the plot of the growth rate of the Fig. 2a (region I). Fig. 4 shows the sequence of plots of phase ϕ_1 in the gray scale (phases $\phi_{2,3}$ look similar but with different orientations). At relatively small times the phase distribution is smooth (Fig. 4a, $t = 200$), however since the directions of the fastest growing disturbances differ from the direction of the primary wavevector \mathbf{q}_1 , the oblique modulation is already seen. As the magnitude of disturbances grows exponentially, at $t \sim 300$ first defects appear (Fig. 4b). At larger times (Fig. 4c, $t = 400$) a metastable state is reached with the phases ϕ_i changing almost linearly in two different directions (making $\pm 120^\circ$ with the directions of \mathbf{q}_i) within large domains separated by grain boundaries. Even at much larger times the pattern is still disordered (see Fig. 4d, $t = 900$). Fig. 5 shows the corresponding plots of the real “temperature” field $T = \sum a_i \exp(i\mathbf{q}_i \cdot \mathbf{r})$ reconstructed from the complex amplitudes a_i . The grain boundaries between the regions with different orientation of hexagons are clearly seen there, and the pattern itself looks very similar to the Turing patterns observed by Ouyang and Swinney in the gel chemical reactor [6]. In Fig. 6 the two-dimensional power spectrum of the complex amplitude A_1 is shown in the logarithmic gray scale for the time $t = 260$. Four distinct maxima at the angles of $\pm\pi/3, \pi \pm \pi/3$ with the direction \mathbf{q}_1 are present in accordance with the linear stability analysis (see Figs. 2a, 3a), although the asymmetry between longer ($\pi \pm \pi/3$) and shorter ($\pm\pi/3$) wave components (a nonlinear effect) is already significant. One can also see many other smaller peaks which result from the nonlinear interaction of primary peaks.

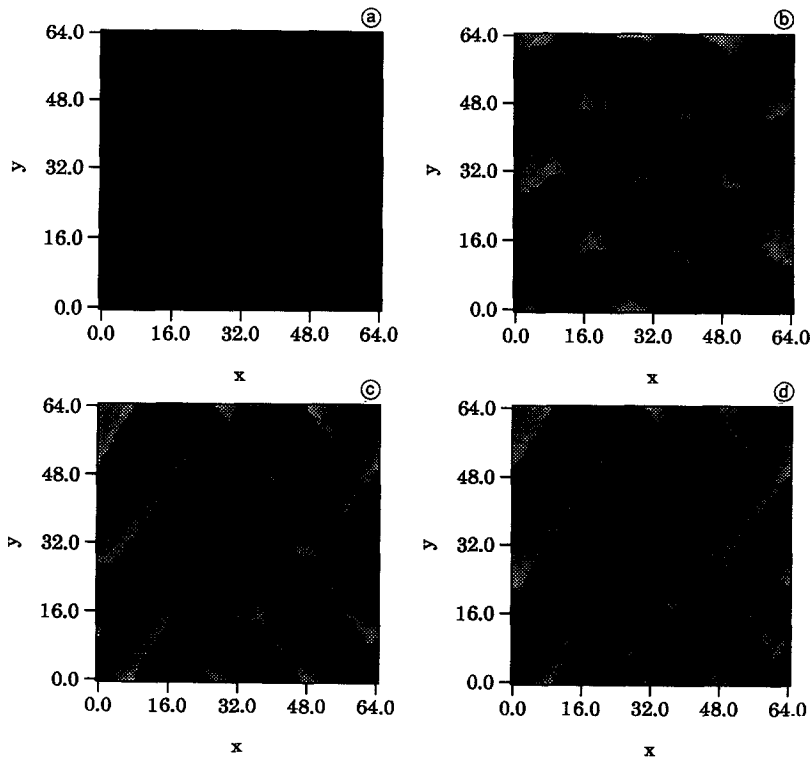


Fig. 4. Evolution of the phase ϕ_1 due to the Eckhaus instability at $K = 0.45$, $\mu = 0.6$ (region I): (a) $t = 200$, (b) $t = 300$, (c) $t = 400$, (d) $t = 900$. Black: $\phi_1 = -\pi$, white: $\phi_1 = \pi$.

Nonlinear dynamics of the Eckhaus instability for the region III ($K = 0.65$, $\mu = 0.6$) looks qualitatively similar to the scenario described above but develop in a much shorter time scale ($t \sim 20$). We do not present the corresponding plots here.

Figs. 7, 8 and 9 demonstrate the evolution of the hexagonal pattern for $K = 0.56$, $\mu = 0.3$. These values of parameters correspond to the region III-A in Fig. 1. As one can see, the domain structure with different orientations of hexagons also emerges here (Figs. 7c, 8c, $t = 60$), however at a later time, a regular hexagonal pattern is restored with smaller wavenumber (Figs. 7d, 8d, $t = 600$)³. Unlike the previous case, the power spectrum (Fig. 10) looks less structured because two modes are unstable, and the global extrema at the angles of $\pm\pi/6$ are only slightly higher than those for $\theta = \pm\pi/3$, in accordance with the linear theory (Section 3, see Fig. 2d).

So far we have considered only rather small μ for which hexagons are the only possible stable state. A completely different final state of the Eckhaus instability is observed for larger $\mu > \mu_*$ where $\mu_* \simeq 1.5$ is some threshold value. It is known that both hexagons and rolls are the stable stationary solutions of Eq. (1) (and, of course, also (2)) in the range

$$\frac{1}{(\gamma - 1)^2} < \mu < \frac{\gamma + 2}{(\gamma - 1)^2} \quad (25)$$

³ It is possible that in the previous case a regular hexagonal pattern would be restored as well, but on a much longer time scale, and we were unable to reach the regular state in our numerical simulations. It is also feasible that the characteristic time of re-ordering grows quickly with the system size.

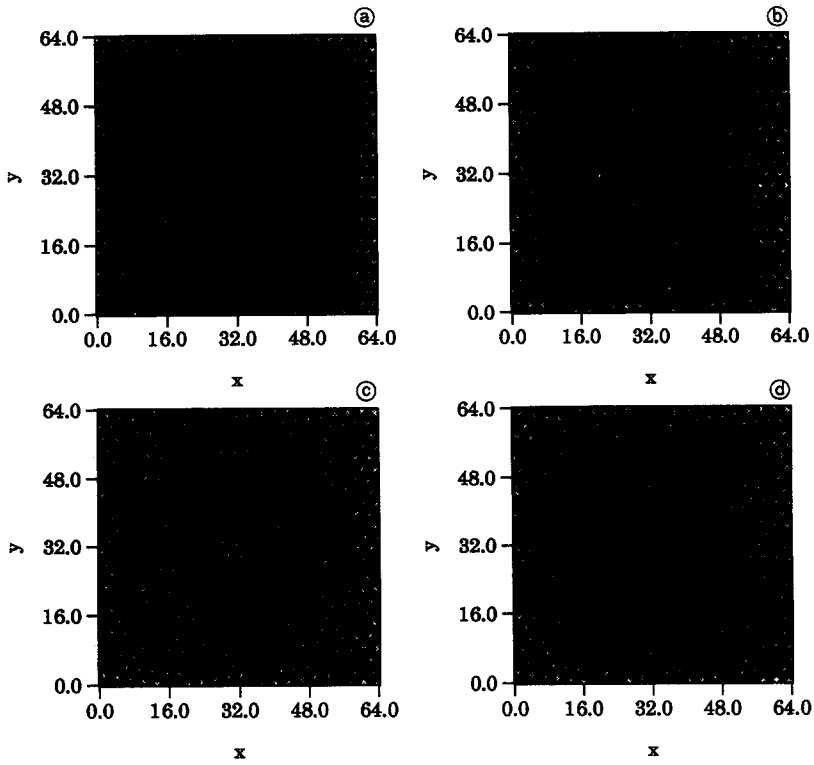


Fig. 5. Evolution of the “temperature” field $T = \sum A_i e^{q_i r} + \text{c.c.}$ under the Eckhaus instability at $K = 0.45$, $\mu = 0.6$ (region I): (a) $t = 200$, (b) $t = 300$, (c) $t = 400$, (d) $t = 900$.

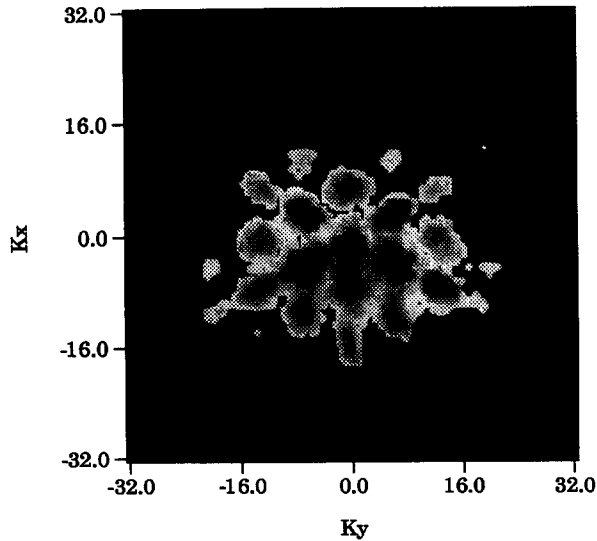


Fig. 6. The power spectrum of the A_1 -field at $t = 260$. At $t = 0$ all the energy was localized at the center ($K_x = K_y = 0$).

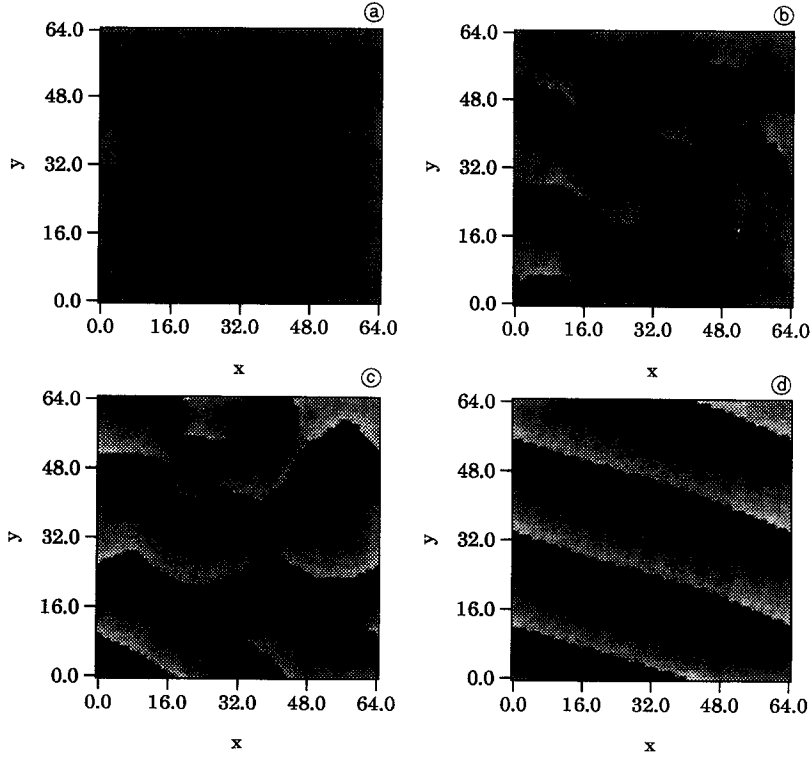


Fig. 7. Evolution of the phase ϕ_1 due to the Eckhaus instability at $K = 0.56$, $\mu = 0.3$ (region III-A): (a) $t = 30$, (b) $t = 40$, (c) $t = 60$, (d) $t = 600$.

(see, for example, [11,12,14,3]). Although at the linear stage of the Eckhaus instability this fact doesn't make a difference, when first defects appear, the dynamics may change. It has been pointed out recently [3] that in the cores of penta-hepta defects of hexagons there are pieces of rolls. Under certain conditions these small domains of roll patterns spread and eventually destroy the hexagonal pattern. The emerging pattern consists of domains with rolls of different orientation. The example of this transition is presented in Fig. 10. The parameter values are $K = 0.6$, $\mu = 1.7$. At $T \sim 50$ the modulation of the initial hexagonal pattern appears (Fig. 10a), at $t = 100$ first defects appear (Fig. 10b), at $t = 260$ the pattern consists of domains of rolls and hexagons with the new wavenumber (Fig. 10c). At larger times $t = 500$ most of hexagonal domain disappear and roll domains prevail (Fig. 10d). Thus, the Eckhaus instability in this case triggers the transition from hexagons to rolls. It is easy to estimate a value of μ_* at which the transition to rolls happens from the energetic considerations. To this end one needs to compare the free energy density for perfect hexagons

$$F_h = -3\mu A_0^2 - 2A_0^3 + \frac{3}{2}(1 + 2\gamma)A_0^4, \quad (26)$$

and for perfect rolls

$$F_r = -\mu A_r^2 + \frac{1}{2}A_r^4, \quad (27)$$

with optimal wavenumber $q = q_0$, where $A_r \equiv \sqrt{\mu}$ is the amplitude of stationary rolls (cf. (3)). It is easy to compute that $F_h = F_r$ at

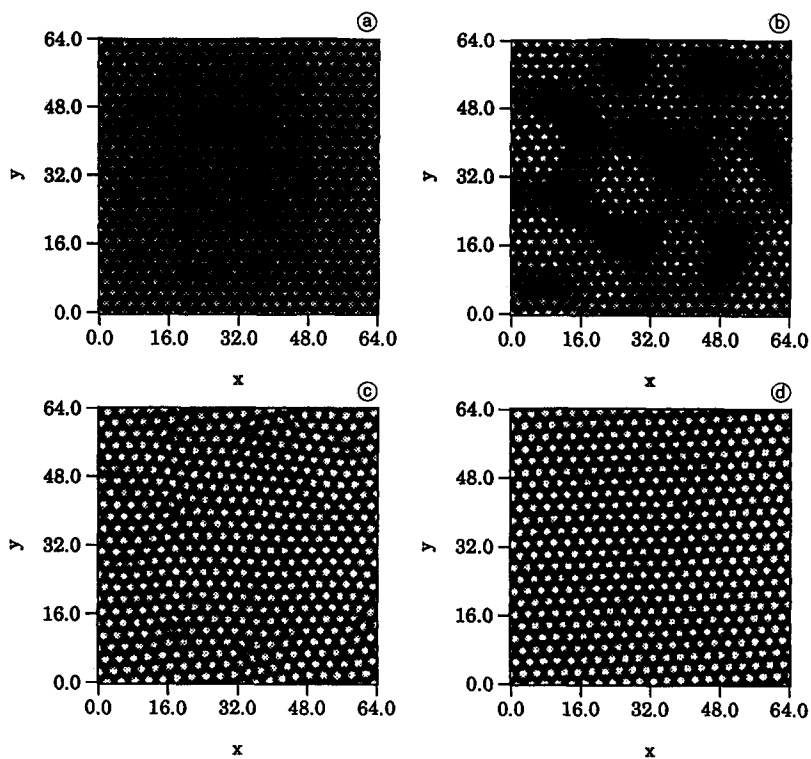


Fig. 8. Evolution of the “temperature” field under the Eckhaus instability at $K = 0.56$, $\mu = 0.3$ (region III-A): (a) $t = 30$, (b) $t = 40$, (c) $t = 60$, (d) $t = 600$.

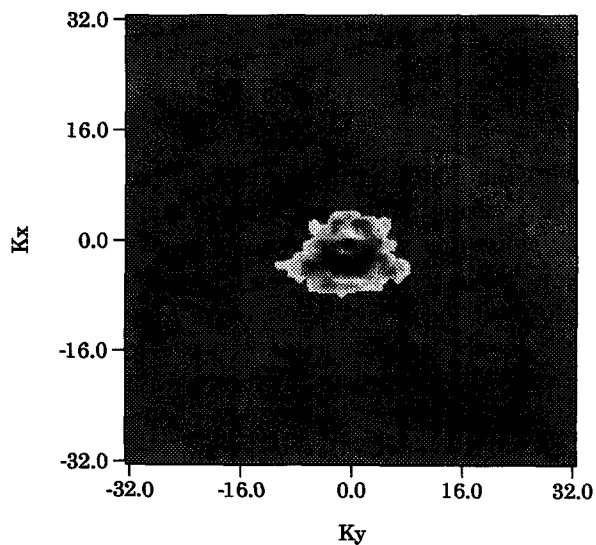


Fig. 9. The power spectrum of the A_1 -field at $t = 55$.

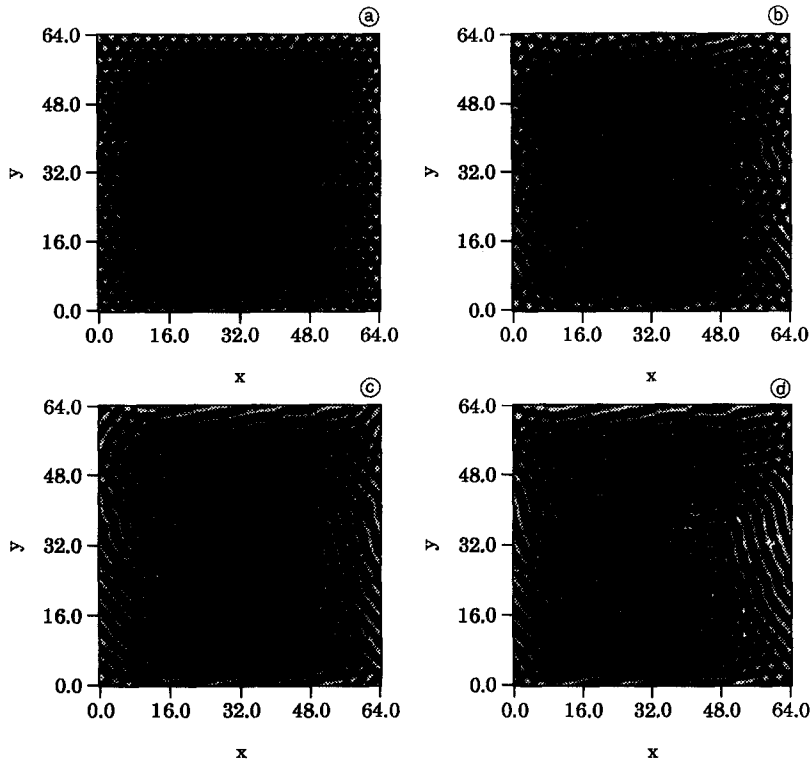


Fig. 10. Evolution of the ‘temperature’ field at $K = 0.6$, $\mu = 1.7$; (a) weak phase modulation of initial hexagonal pattern ($t = 55$), (b) first defects with inclusions of roll state appear ($t = 100$), (c) disordered roll-hexagon state ($t = 260$), (d) asymptotic state of the system ($t = 500$). The hexagonal phase is seen at the domain walls separating the roll patterns with different orientation.

$$\mu_* = \frac{3\gamma + 1 + \sqrt{2}(\gamma + 1)^{3/2}}{2(1 + 2\gamma)(\gamma - 1)^2}, \quad (28)$$

which of course coincides with the condition for immobility of roll–hexagon domain walls [17]. For $\gamma = 2$, $\mu_* = 1.4348 \dots$. This value slightly underestimates the real threshold of the hexagon–roll transition in our simulations since this simple energetic analysis does not take into account the nonuniform structure of defects. Nevertheless, it is in a reasonable agreement with numerical results.

As we have mentioned before, at the intermediate stage a number of walls separating domains with different orientation of rolls appear. The angle between rolls is close to $\pi/3$, so the domain walls should be ‘resonant’ (a term from Ref. [17]) in a sense that these two rolls would generate the third roll pattern in the overlapped region, and therefore a thin layer of hexagonal phase remains sandwiched at the wall. These hexagonal domain walls are indeed observed, especially if $\mu \sim \mu_*$ (see Fig. 10c,d). This agrees with the conclusion of Ref. [17] that the width of the resonant domain wall $\delta \sim -\ln(\mu - \mu_*)$ at small $(\mu - \mu_*)$.

Let us remark in the conclusion of this section that the Eckhaus (or cross-roll) instability of rolls may also trigger the backward transition from roll to hexagons if $(\gamma - 1)^{-2} < \mu < \mu_*$, and initially the rolls with non-optimal wavenumber are present.

5. Conclusions

In this paper we investigated the Eckhaus instability of hexagonal patterns. We employed the amplitude equations, which make the conclusions insensitive to the specific physical nature of the system. Using a phase approximation we found the stability limits in the (K, μ) parameter plane. Unlike the case of rolls, the region of stability for hexagons is closed. Within the full set of the linearized amplitude equations we found the structure of growing disturbances and predicted a symmetry breaking at the nonlinear stage of the instability. Our numerical simulations confirmed that prediction. Depending on the parameters, “narrow” or “wide” splitting of the initial triplet of rolls happens and domains with different orientations of hexagons emerge, separated by numerous line and point defects. These defects interact with each other, and after a long time evolution, a new regular hexagonal pattern may form. For larger $\mu > \mu_*$ the Eckhaus instability triggers the transition from regular hexagonal pattern with non-optimal wavenumber to a disordered state of rolls with wavenumber close to optimal and different orientation inside different domains.

We did not dwell upon the case of negative K which corresponds to the hexagonal pattern with the wavelength larger than the optimal one. In the case of $\alpha \rightarrow 0$ we considered here, only the absolute value of K is significant. Our preliminary numerical simulations with small but finite $\alpha/q_0 = \mathcal{O}(10^{-1})$ show that qualitatively the same scenario of the Eckhaus instability is observed, and no long-wave “zig-zag”-type instability occurs. However, the difference between positive and negative K might be important in the range of the cross-hexagon instability, which is beyond the scope of the amplitude description we adopted here.

We believe that the model of envelope equations we used here captures qualitatively the effects in real physical situations like non-Boussinesq thermal convection. However, analysis of more realistic models like the generalized Swift–Hohenberg equation with mean flow taken into account [18] is needed for more detailed predictions and quantitative comparison with a specific experiment.

When the work on this paper was in progress, we became aware that Walgraef has been studying a similar problem [19].

Acknowledgements

Authors thank K. Eaton for reading an early version of the manuscript and useful comments. The support of the U.S. Department of Energy Contract No.DE-FG03-90ER14138, ARPA Contract No.92-F141900-000, and of the Office of Naval Research Contract N00014-D-0142 DO#15 is gratefully acknowledged.

References

- [1] R.W. Walden and G. Ahlers, *J. Fluid. Mech.* 109 (1981) 89.
- [2] S. Ciliberto, E. Pampaloni and C. Perez-Garcia, *Phys. Rev. Lett.* 61 (1988) 1198.
- [3] S. Ciliberto, P. Couillet, J. Lega, E. Pampaloni and C. Perez-Garcia, *Phys. Rev. Lett.* 65 (1990) 2370.
- [4] P. Cerisier, C. Perez-Garcia, C. Jamond and J. Pampaloni, *Phys. Rev. A* 35 (1987) 1949.
- [5] Q. Ouyang and H.L. Swinney, *Nature* 352 (1991) 610.
- [6] J. Verdasca, A. de Wit, G. Dewel and P. Borckmans, *Phys. Lett. A* 168 (1992) 194.
- [7] M. Cross and P. Hohenberg, *Rev. Modern Phys.* 65 (1993) 851.
- [8] H. Haken, *Advanced Synergetics* (Springer, New York, 1983).
- [9] H.R. Brand, *Progr. Theor. Phys. Suppl.* 99 (1989) 442.

- [10] V. Eckhaus, *Studies in Nonlinear Stability Theory* (Springer, Berlin, 1965).
- [11] L.A. Segel, *J. Fluid Mech.* 21 (1965) 359.
- [12] F. Busse, *J. Fluid Mech.* 30 (1967) 625.
- [13] B. Caroli, C. Caroli and B. Roulet, *J. Crystal Growth* 68 (1984) 677.
- [14] B.A. Malomed and M.I. Tribelski, *Sov. Phys. -JETP* 65 (1987) 305.
- [15] A.C. Newell and J.A. Whitehead, *J. Fluid Mech.* 38 (1969) 279;
L.A. Segel, *J. Fluid Mech.* 38 (1969) 203.
- [16] F. Busse and J.A. Whitehead, *J. Fluid Mech.* 66 (1971) 67.
- [17] B.A. Malomed, A.A. Nepomnyashchy and M.I. Tribelsky, *Phys. Rev. A* 42 (1990) 7244.
- [18] H.S. Greenside, M.C. Cross and W.M. Coughran, Jr. *Phys. Rev. Lett.* 60 (1988) 2269.
- [19] D. Walgraef, Report at the NATO Advanced Research Workshop “Spatio-Temporal Patterns in Nonequilibrium Complex Systems”, April 13–17, 1993, Santa Fe.